RSC Advances

PAPER

View Article Online
View Journal | View Issue

Cite this: *RSC Adv.*, 2019, **9**, 4834

Preparation, crystal structure and luminescence properties of a novel single-phase red emitting phosphor $CaSr_2(PO_4)_2:Sm^{3+},Li^+$†

Yuying Chen,[ab] Qingfeng Guo,*[ab] Libing Liao,*[c] Mingyue He,[ab] Tianshuai Zhou,[c] Lefu Mei,*[c] Marcin Runowski[d] and Bin Ma[e]

Received 11th January 2019
Accepted 2nd February 2019

DOI: 10.1039/c9ra00264b

rsc.li/rsc-advances

Single-phase $CaSr_2(PO_4)_2:Sm^{3+},Li^+$ phosphors were prepared *via* a high-temperature solid-state method under air. The powder X-ray diffraction patterns, scanning electron microscopy images, photoluminescence spectra, and concentration-dependent emission spectra were measured to characterize the as-prepared phosphors and luminescence decay curves. The results showed that the $CaSr_2(PO_4)_2:Sm^{3+},Li^+$ phosphors exhibited red luminescence, and the emission spectra of the phosphors consisted of four sharp peaks at around 565, 601 (the strongest one), 647 and 707 nm. The optimum doping concentration of Sm^{3+} ions was 0.09 (mol concentration), and the mechanism of energy transfer among Sm^{3+} ions was defined to be quadrupole–quadrupole (q–q) interactions using Dexter's theory. The Blasse concentration quenching method was used to determine the critical distance R_c for energy transfer among Sm^{3+} as 10.99 Å. The results indicate that the as-prepared phosphors have good thermal stability with an activation energy of 0.773 eV *via* temperature-dependent emission spectra. Therefore, $CaSr_{2-2x}(PO_4)_2:xSm^{3+},xLi^+$ materials can be used as red-emitting phosphors for UV-pumped white-light emitting diodes.

1. Introduction

High efficiency, long-life and non-polluting light sources are urgently needed.[1,2] In contrast to traditional lighting sources, white light emitting diodes (w-LEDs) offer high energy conversion efficiency, small volume, low starting voltage, long durability and good color rendering.[3–5] Phosphors are an important component of LEDs, but have a poor color rendering index when used in w-LEDs. Multi-phosphor mixing usually results in color imbalance and instability at higher temperatures, effectively limiting their applications. Therefore, new high efficiency phosphor systems are needed to improve the luminous efficiency of LEDs—especially those excited by near ultraviolet or blue chips. Lanthanides have transitions between 5d → 4f and 4f → 4f, leading to tunable multicolor luminescence in the UV-Vis-NIR range, long radiative lifetimes, and narrow absorption and emission bands; thus, lanthanides are very important in the display and lighting fields.[6–8] Red or orange-red emitting phosphors can be prepared *via* appropriate doping of the selected materials with lanthanide ions, *i.e.* Eu^{3+} or Sm^{3+}. Compared with Eu^{3+}-doped materials, Sm^{3+}-doped phosphors can be easily excited in the blue region, which is useful for excitation in the near-ultraviolet (n-UV) InGaN-based LED chip (350–420 nm).[9] Moreover, the use of Sm^{3+} ions is much more cost-effective than very expensive Eu^{3+} ions.

Whitlockite has a chemical formula $M_3(PO_4)_2$ (M = Ca, Sr, Ba) and has been investigated as a potential host for luminescent materials.[10–12] $CaSr_2(PO_4)_2$ belongs to whitlockite, and it can be a suitable host, for phosphors due to its excellent luminescence properties.[13] However, research into the luminescence properties and structure characteristics of Sm^{3+} doped $CaSr_2(PO_4)_2$ is rare. Here, a novel Sm^{3+} doped $CaSr_2(PO_4)_2$ phosphor was prepared for the first time, and its luminescence and crystal structures were investigated in detail.

Here, a series of the $CaSr_{2-2x}(PO_4)_2:xSm^{3+},xLi^+$ phosphors were synthesized by a high-temperature solid-state reaction method in air atmosphere, for the first time. The samples were characterized by X-ray diffraction (XRD), scanning electron microscopy (SEM), photoluminescence excitation (PLE) and

[a]School of Gemology, China University of Geosciences, Beijing 100083, China. E-mail: qfguo@cugb.edu.cn
[b]Jewelry and Mineral Materials Laboratory of Experimental Teaching Demonstration Center, Beijing, China
[c]Beijing Key Laboratory of Materials Utilization of Nonmetallic Minerals and Solid Wastes, National Laboratory of Mineral Materials. School of Materials Sciences and Technology, China University of Geosciences, Beijing 100083, China. E-mail: clayl@cugb.edu.cn; mlf@cugb.edu.cn
[d]Adam Mickiewicz University, Faculty of Chemistry, Department of Rare Earths, Umultowska 89b, 61-614 Poznań, Poland
[e]Qinghai Provincial Key Laboratory of New Light Alloys, Qinghai Provincial Engineering Research Center of High Performance Light Metal Alloys and Forming, Qinghai University, Xining 810016, PR China

† Electronic supplementary information (ESI) available. See DOI: 10.1039/c9ra00264b

emission (PL) spectra, and decay curves. The XRD pattern of the $CaSr_2(PO_4)_2$ phase is similar to whitlockite mineral, which crystallizes in the space group *R*3*c*. In addition, the as-prepared phosphors have good thermal stability *via* temperature-dependent emission spectra. The results indicate, that the as-prepared $CaSr_2(PO_4)_2$:Sm^{3+},Li^+ phosphor can act as a UV convertible, red phosphor for w-LEDs.

2. Experimental section

2.1. Materials and synthesis

The $CaSr_{2-2x}(PO_4)_2$:xSm^{3+},xLi^+ ($x = 0$–0.3) powder samples were synthesized *via* high temperature solid-state method. The starting materials, $CaCO_3$ (99.9%), $SrCO_3$ (99.9%), Li_2CO_3 (99.9%), $(NH_4)_2HPO_4$ (99.9%), and Sm_2O_3 (99.999%) were purchased from Aldrich. First, according to the stoichiometric ratios, these starting materials were mixed and thoroughly ground in an agate mortar. The pre-sintered samples were then evenly transferred to a tube furnace at 800 °C for 1 h of decomposition of the calcium carbonate and strontium carbonate in air. Finally, the as-prepared powders were calcined at 1250 °C for 5 h in air atmosphere, and the furnace was cooled down to room temperature before their removal.

2.2. Characterization

A series of the obtained $CaSr_{2-2x}(PO_4)_2$:xSm^{3+},xLi^+ phosphors were measured by XRD analysis (XD-3, PGENERAL, China) in the 2θ range of 10° to 70°, with Cu Kα radiation ($\lambda = 0.15406$ nm) operating at 40 kV and 40 mA. The step scanning rate (2θ values ranging from 5° to 120°) used for Rietveld analysis was 1 s per step with a step size of 0.02°. The PL and PLE spectra of the phosphors were measured on a F-4600 spectrofluorometer (HITACHI, Japan) with a photomultiplier tube operating at 500 V, and a 150 W Xe lamp used as an excitation source. A 400 nm cut-off filter was used to eliminate the second-order emission. The temperature-dependent PL spectra were also measured on the same spectrofluorometer with a home-made heating controller. The $CaSr_2(PO_4)_2$ were observed by SEM using a HitachiS-520 instrument. The X-ray photoelectron spectroscopy (XPS, ESCALab250, Thermo Scientific, America) with monochromatic 150 W Al Kα radiation was used to detect Sm^{3+}. The room-temperature luminescence decay curves were recorded with a spectrofluorometer (Horiba, JobinYvon TBXPS), using a tunable pulse laser radiation as the excitation source.

3. Results and discussion

3.1. Crystal structure

The valence charge is imbalanced when M^{n+} ions were substituted by $M^{(n+1)}$. This is undesirable for the phosphor materials and decreases the luminescence intensity. To avoid the charge unbalance and the formation of vacancy in the sample, the Li^+ ions were employed as charge compensators and added along with the Sm^{3+} ions. The mechanism of charge compensation is that two Sr^{2+} ions are replaced by one Sm^{3+} ion and one Li^+ ion. Therefore, the crystallinity of $CaSr_2(PO_4)_2$:Sm^{3+},Li^+ improves because the doping with Li^+ lowers the crystallization temperature. The XRD patterns of the synthesized $CaSr_{2-2x}(PO_4)_2$:xSm^{3+},xLi^+ (x = 0.01, 0.06, 0.09, 0.12, 0.15, and 0.18) are shown in Fig. 1. The XRD patterns of the synthesized $CaSr_{2-1.5x}(PO_4)_2$:xSm^{3+}, (x = 0.01, 0.03, 0.05, 0.07, 0.09, 0.12, 0.15 and 0.18) and $CaSr_2(PO_4)_2$ are shown in Fig. 2. The introduction of Li^+ did not have any significant influence on the structure of the as-prepared samples. All XRD patterns can be well fitted with the standard patterns of the $Ca_3(PO_4)_2$ (JCPDS no. 09-0169) belonging to the trigonal crystal system, with a space group of *R*3*c* (161). This suggests that all samples are crystallized in the single phase. All diffraction peaks shifted to the smaller 2θ angle side (bigger *d*-spacing, *i.e.*, interplanar distances), which can be ascribed to the substitution of Ca^{2+} by bigger Sr^{2+}. The Sm^{3+} and Li^+ ions have been successfully

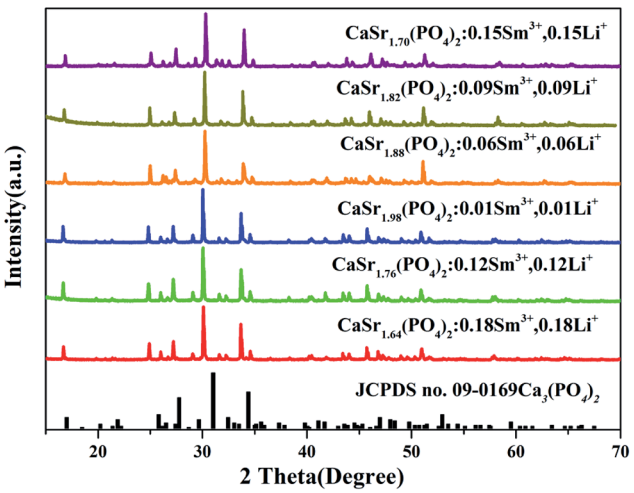

Fig. 1 The XRD patterns of $CaSr_{2-2x}(PO_4)_2$:xSm^{3+},xLi^+ phosphors (x = 0.01, 0.03, 0.06, 0.09, 0.12, 0.15, 0.18, 0.24, 0.27 and 0.3) and the standard pattern of $Ca_3(PO_4)_2$ (JCPDS no. 09-0169) is shown as a reference.

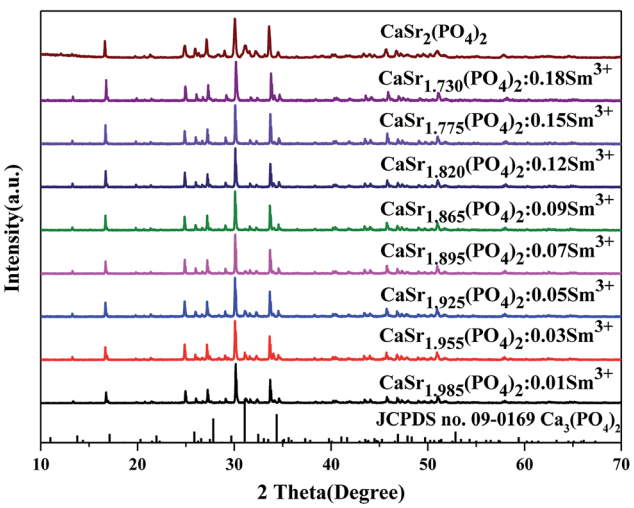

Fig. 2 The XRD patterns of $CaSr_{2-2x}(PO_4)_2$:xSm^{3+} phosphors (x = 0, 0.01, 0.03, 0.05, 0.07, 0.09, 0.12, 0.15 and 0.18) and the standard pattern of $Ca_3(PO_4)_2$ (JCPDS no. 09-0169) is shown as a reference.

embedded into the crystal lattice-the Sm^{3+} and Li^{+} dopant ions have no obvious influence on the structure of the host $CaSr_2(PO_4)_2$ at various doping amounts. In order to further detect the phase purity of the phosphors, the $CaSr_{1.82}Sm_{0.09}Li_{0.09}(PO_4)_2$ was selected for refinements. Fig. S1† shows the Rietveld refinement of $CaSr_{1.82}Sm_{0.09}Li_{0.09}(PO_4)_2$ by TOPAS program. Solid red lines are calculated intensities, and blue circles are the observed intensities. Short orange vertical lines show the position of Bragg reflections of the calculated pattern. Green solid lines below the profiles stand for the difference between the observed and the calculated intensities. Refinement was stable and gives low *R*-factors (Table S1 and Fig. S1†). All the experimental peaks were well fitted by the refinement, indicating that all those peaks are Bragg reflections from the whitlockite structure. The lattice parameters of the phosphor are determined to be $a = b = 10.5918(11)$ Å, $c = 38.835(4)$ Å and $V = 3773.06(55)$ Å^3, respectively. The lattice parameters of the phosphor were a little different from $Ca_3(PO_4)_2$, which was caused by the isomorphic substitution. The refined atomic positions and isotropic temperature factors for all atoms are also shown in Table S2.†

Fig. 3 shows the crystal structure of $CaSr_2(PO_4)_2$ and different coordination environment for Ca/Sr atoms. The crystal structure of the $CaSr_2(PO_4)_2$ is a result of the lattice deformation of $Ca_3(PO_4)_2$, *via* partial substitution of Ca^{2+} with Sr^{2+}. In the crystal structure of the $CaSr_2(PO_4)_2$, the Ca^{2+}/Sr^{2+} ions are distributed between five crystallographic sites—all of these are occupied by both Ca^{2+} and Sr^{2+} ions in different ways. The Sr1/Ca1, Sr2/Ca2, Sr3/Ca3, Sr4/Ca4 and Sr5/Ca5 positions are coordinated with six, six, seven, three and six oxygen atoms, respectively.[14] Of note, the Ca4 is threefold coordinated, suggesting weak bonding and the formation of crystal defects.

To investigate the composition and morphology of the material, the $CaSr_{1.82}(PO_4)_2$:0.09Sm^{3+},0.09Li^{+} phosphor was selected as a representative example for measurements. Fig. 4(a) displays the elemental analysis result of the sample measured

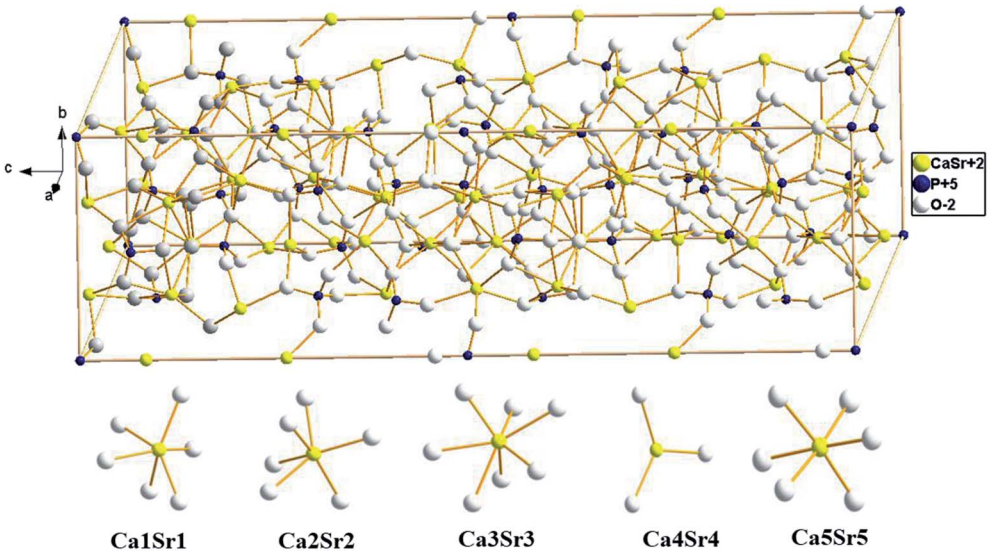

Fig. 3 Crystal structure of the host $CaSr_2(PO_4)_2$ compound, showing different coordination environment for Ca/Sr atoms.

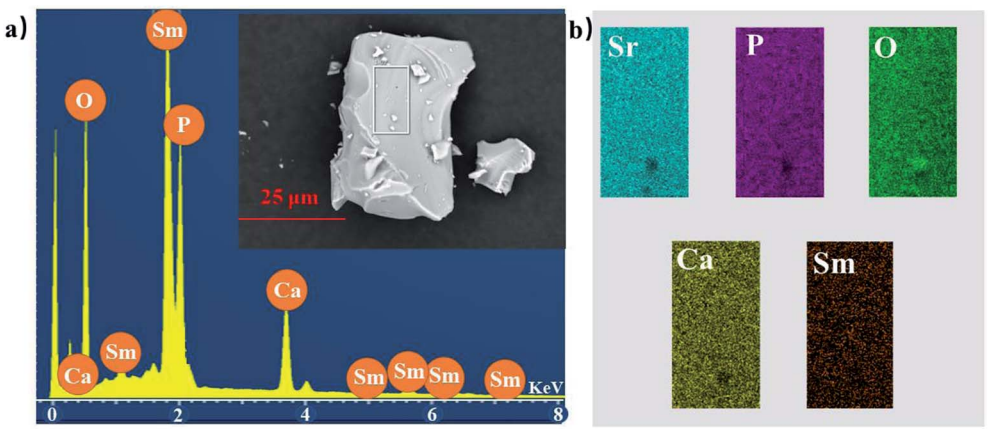

Fig. 4 (a) The elemental analysis result of the sample measured by the EDS method, within the red rectangle area and the inset showing the SEM image of the $CaSr_{1.82}(PO_4)_2$:0.09Sm^{3+},0.09Li^{+} sample. (b) The elemental mapping of $CaSr_{1.82}(PO_4)_2$:0.09Sm^{3+},0.09Li^{+} phosphors.

by the EDS method, within the red rectangle area; the inset shows SEM images of the $CaSr_{1.82}(PO_4)_2$:0.09Sm^{3+},0.09Li^+ sample with elemental mapping of $CaSr_{1.82}(PO_4)_2$:0.09-Sm^{3+},0.09Li^+ phosphor provided in Fig. 4(b). The EDS results indicate that the synthesized phosphor is composed of Ca, Sr, P, O, and Sm, which is consistent with the composition of $CaSr_{1.82}(PO_4)_2$:0.09Sm^{3+},0.09Li^+ material. The SEM image reveals that the as-prepared samples are well-crystallized. The sample consists of irregular crystal sizes (≈1000–2000 nm).

The Sm 3d core level X-ray photoelectron spectra (XPS) of $CaSr_{1.82}(PO_4)_2$:0.09Sm^{3+},0.09Li^+ were measured to confirm the existence of Sm^{3+}, as shown in Fig. 5. These data indicate the existence of trivalent oxidation states of Sm on the sample's surface. Only Sm^{3+} can be found; no peaks of Sm^{2+} can be seen. The XPS results are consistent with the EDS results.

3.2. Photoluminescence properties

Fig. 6 shows the PLE spectra of the $CaSr_{2-2x}(PO_4)_2$:xSm^{3+},xLi^+ (x = 0.01–0.3) phosphors monitored at 601 nm and room temperature. All PLE spectra have strong and narrow absorption bands ranging from 250 to 550 nm in the UV and visible range. These are ascribed to the intrinsic $4f^5$–$4f^5$ transitions of Sm^{3+} ions.[15] The observed peaks around 305, 318, 333, 345, 375, 391, 403, 416, 440, 466 and 477 nm, correspond to the transitions from the ground level $^6H_{5/2}$ to the excited levels $^4P_{5/2}$, $^4P_{3/2}$, $^4G_{7/2}$, $^4D_{7/2}$, $^6P_{7/2}$, $^2L_{15/2}$, $^4F_{7/2}$, $^6P_{5/2}$, $^4M_{17/2}$, $^4H_{13/2}$, and $^4I_{11/2}$ of Sm^{3+}, respectively.[16–18] The most intense band in the PLE spectra is located at 403 nm, in the near-UV region.

Fig. 7 depicts the PL spectra of the $CaSr_{2-2x}(PO_4)_2$:xSm^{3+},xLi^+ (x = 0.01–0.3) phosphors measured at room temperature excited at 403 nm ($^6H_{5/2} \rightarrow {}^4F_{7/2}$); the inset shows the dependence of the emission intensity at 707, 647, 601, and 565 nm on the Sm^{3+} doping concentration.

All PL spectra exhibit similar profiles with four emission peaks typical of Sm^{3+}, associated with $^4G_{5/2} \rightarrow {}^6H_J$ (J = 5/2, 7/2, 9/2, 11/2) transitions in Sm^{3+} ions.[19,20] The inset in Fig. 7 shows the dependence of emission intensity on the Sm^{3+} doping concentration at 565, 601, 647, and 707 nm corresponding to the electronic transitions of $^4G_{5/2} \rightarrow {}^6H_{5/2}$, $^4G_{5/2} \rightarrow {}^6H_{7/2}$, $^4G_{5/2} \rightarrow {}^6H_{9/2}$, and $^4G_{5/2} \rightarrow {}^6H_{11/2}$, respectively.[15] In addition, the $^4G_{5/2} \rightarrow {}^6H_{7/2}$ transition (at 601 nm) is the strongest one. There are no significant variations in the emission band positions or shape in any phosphor. The inset of Fig. 7 shows that the emission intensities at 565, 601, 647, and 707 nm increase with the concentration of Sm^{3+} ions. They then reach a maximum when the concentration of Sm^{3+} is 0.09. Finally, they decrease with further increases in Sm^{3+} content which corresponds to the concentration quenching effect.[21] The quantum efficiency of the $CaSr_{1.82}(PO_4)_2$:0.09-Sm^{3+},0.09Li^+ phosphor is 9.23%.

Fig. 8(a) shows the emission spectra of $CaSr_2(PO_4)_2$:0.03-Sm^{3+},xLi^+ (x = 0.01, 0.02 and 0.03) phosphors and the emission spectra of $CaSr_2(PO_4)_2$:0.03Sm^{3+},xNa^+(x = 0.01) under 403 nm excitation. The emission spectra of $CaSr_2(PO_4)_2$:0.03Sm^{3+},Li^+/Na^+ samples include some peaks centered at 565, 601, 647 and 707 which are similar to those mentioned in Fig. 7. The inset shows the dependence of the emission intensity at 601 nm on the Li^+/Na^+ doping concentration. This indicates that Li^+ enhances the luminescent intensity of phosphors and is more effective than Na^+. Fig. 8(b) illustrates the emission spectra of $CaSr_{2-1.5x}(PO_4)_2$:xSm^{3+}, (x = 0.03–0.18) phosphors, and the inset shows the dependence of the emission intensity at 601 nm on the Sm^{3+} doping concentration. We see that the luminescence trend of the phosphor at 601 nm is similar to that shown in Fig. 7. The luminescence increases with increasing concentration of Li^+ ions. The maximum luminescence intensity is achieved at 3% Li^+ doping content. The phosphors need to produce ion defects to maintain the charge balance because the replacement of Sr^{2+} with Sm^{3+} is not equal. However, too many defects produce crystal lattice distortions that reduce the luminescence intensity. The excess positive charge from Li^+ ions can be compensated by ion defects according to the following formula: $2Sr^{2+} = Sm^{3+} + Li^+$. This enhances luminescence intensity. There is also an effect on the change in asymmetry. It is reasonable to assume that the Li^+ doping changed the local environment of crystal field reducing the local environment symmetry, which in turn enhanced the emission intensity.

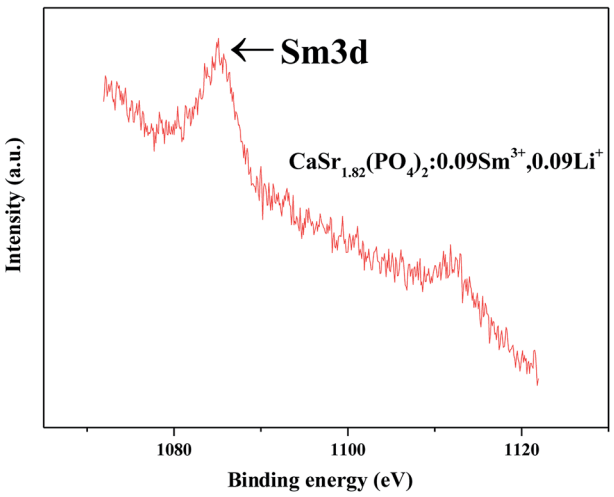

Fig. 5 Sm 3d core level X-ray photoelectron spectra (XPS) of $CaSr_{1.82}(PO_4)_2$:0.09Sm^{3+},0.09Li^+.

3.3. Energy transfer mechanism

It is well-known that the decrease in the photoluminescence intensity is mainly due to the concentration quenching of Sm^{3+} ions, which is usually caused by the cross-relaxation energy transfer between Sm^{3+} ions.[22] The critical distance R_c for the energy transfer between Sm^{3+} ions can be estimated using the following equation proposed by Blasse:[23]

$$R_c \approx 2\left[\frac{3V}{4\pi x_c N}\right]^{1/3}, \quad (1)$$

in which V stands for the volume of the unit cell, x_c is the critical concentration of activator ion (Sm^{3+}) beyond concentration quenching, and N represents the number of host cations in one unit cell. In our case, N = 10, V was estimated to be 626.5 Å, and x_c

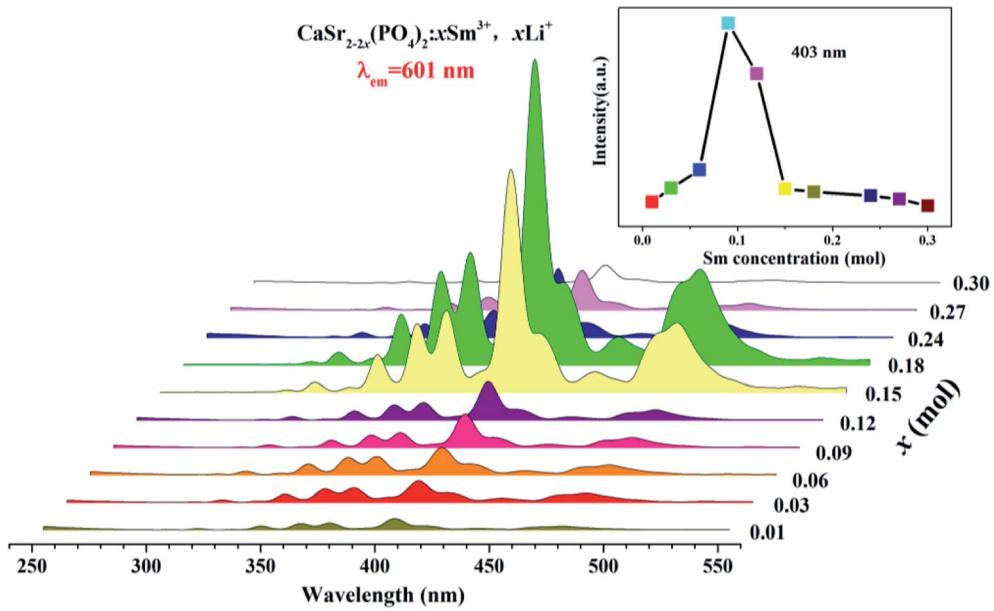

Fig. 6 The PLE spectra of the $CaSr_{2-2x}(PO_4)_2$:xSm^{3+},xLi^+ ($x = 0.01$–0.3) phosphors, measured at room temperature and monitored at 601 nm; the inset shows the dependence of the excitation intensity at 403 nm on the Sm^{3+} doping concentration.

is 0.09 according to the above discussions. According to eqn (1), R_c was turned to 10.99 Å ($x_c = 0.09$). It is well-known that exchange interactions play a vital role in the energy transfer mechanism when the critical distance between the sensitizer and the activator ions is less than 4 Å. With a much bigger R_c value, the energy transfer mechanism is considered to be an electric multipolar interaction. Based on Dexter's theory, if the energy transfer occurs by electric multipolar interactions, then the relationship between the luminescent intensity (I) and the activator concentration (x) can be expressed by the following equation:[24]

$$\frac{1}{x} = K\left[1 + \beta(x)^{\frac{\theta}{3}}\right]^{-1} \quad (2)$$

Here x is the activator concentration, and θ is a multipolar interaction constant equal to 3, 6, 8 or 10 corresponding to the nearest-neighbor ions, *i.e.*, dipole–dipole (d–d), dipole–

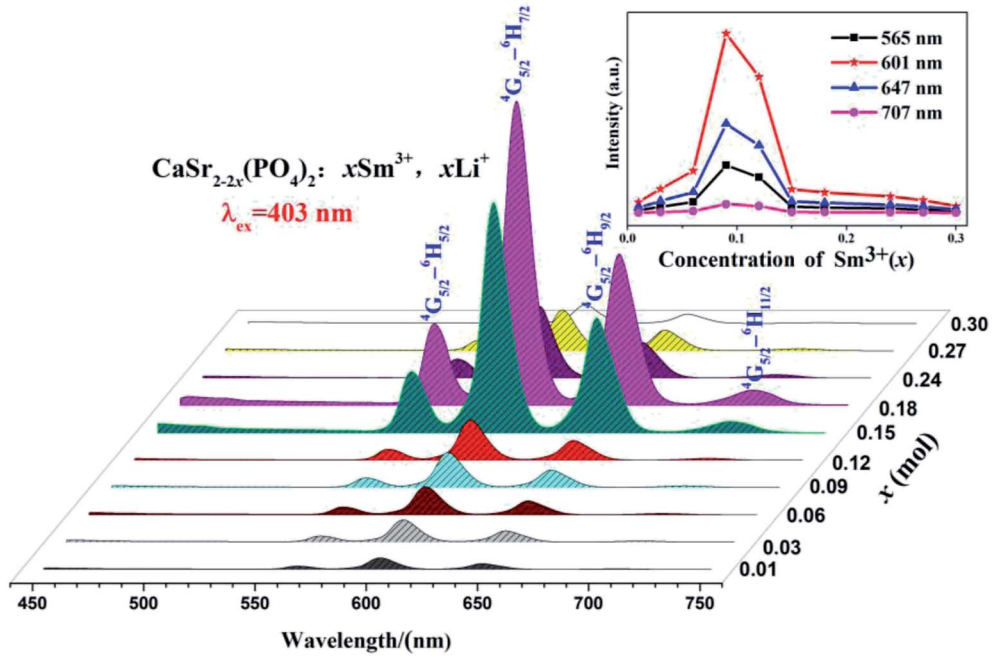

Fig. 7 The PL spectra of the $CaSr_{2-2x}(PO_4)_2$:xSm^{3+},xLi^+ ($x = 0.01$–0.3) phosphors, measured at room temperature with the excitation of 403 nm ($^6H_{5/2} \rightarrow {}^4F_{7/2}$); the inset shows the dependence of the emission intensity at 707, 647, 601 and 565 nm on the Sm^{3+} doping concentration.

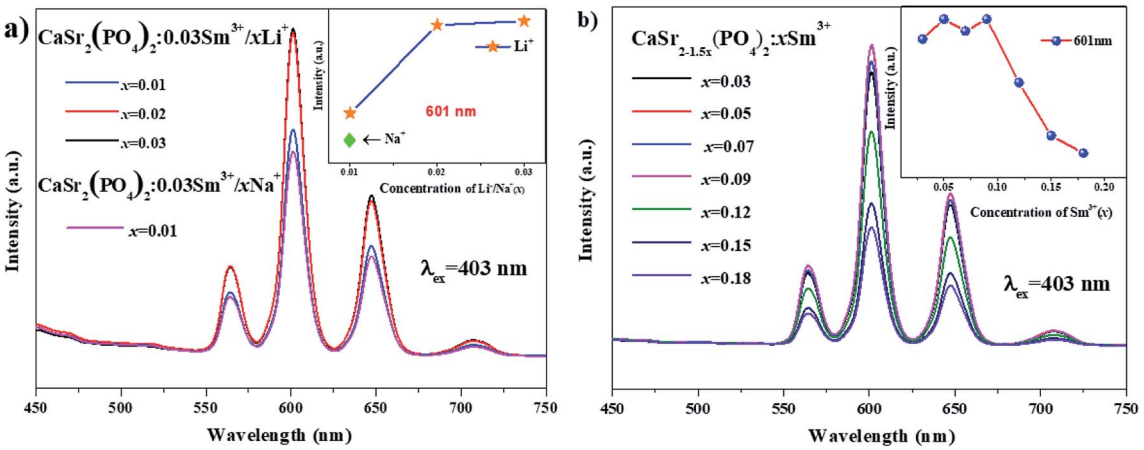

Fig. 8 (a) The emission spectra of $CaSr_2(PO_4)_2$:0.03Sm^{3+},xLi^+ (x = 0.01, 0.02 and 0.03) phosphors and the emission spectra of $CaSr_2(PO_4)_2$:0.03Sm^{3+},xNa^+(x = 0.01); the inset shows the dependence of the emission intensity at 601 nm on the Li^+/Na^+ doping concentration. (b) The emission spectra of $CaSr_{2-1.5x}(PO_4)_2$:xSm^{3+} (x = 0.03–0.18) phosphors; the inset shows the dependence of the emission intensity at 601 nm on the Sm^{3+} doping concentration.

quadrupole (d–q), and quadrupole–quadrupole (q–q) interactions, respectively,[25] Terms K, β are constants for each interaction at the same excitation.[26] Exceeding the quenching concentration, we chose the $CaSr_{1.82}(PO_4)_2$:0.09Sm^{3+}, 0.09Li^+ samples for the constant emission intensity measurements at 601 nm. The relation of log(I/x) *vs.* log(x) for the $CaSr_{2-2x}(PO_4)_2$:xSm^{3+},xLi^+ (x = 0.12, 0.15, 0.18, 0.24, 0.27 and 0.3) of the peaks at 565, 601, 647 and 707 nm were plotted and depicted in Fig. 9. All θ values are close to 10, which means that the quenching mechanism between Sm^{3+} ions in the $CaSr_2(PO_4)_2$ samples belongs to quadrupole–quadrupole (q–q) interactions.

3.4. Temperature-dependent luminescent properties

The thermal stability of the phosphor is a key issue for high-power w-LEDs because the luminescence intensity for most phosphors decreases if the operating temperature exceeds a certain value, *i.e.*, temperature quenching.[27] Fig. 10 shows the temperature-dependent emission spectra of the $CaSr_{1.82}(PO_4)_2$:0.09Sm^{3+},0.09Li^+ phosphor from 298 to 523 K with 403 nm excitation; the inset shows the relative emission intensities at 565, 601, 647, and 707 nm as a function of temperature. The shape of the emission bands remains nearly constant with increasing temperature (Fig. 10) suggesting that the phosphor has excellent color stability, which is crucial in LEDs or high temperature LEDs. However, with increasing temperature (from 300 to 350 K), the emission peaks centered at 565, 601, 647, and 707 nm first slightly increase. These emission intensities decrease gradually when the temperature exceeds 350 K. In contract to typical luminescence thermal quenching where the emission intensity decreases with increasing temperature, the emission characteristics of the obtained Sm^{3+}-doped phosphors exhibit abnormal thermal quenching in the temperature range of 300–350 K (λ_{ex} = 403 nm). This abnormal thermal quenching phenomenon has also been found previously in the literature.[28] We assume that the energy transfer or temperature dependence of absorption coefficient might lead to this abnormal thermal quenching. When the temperature is higher than 350 K, the decrease in PL intensities is due to the temperature-dependence of the electron–phonon interactions in both the ground and excited states of the luminescence center. The emission intensity of the $CaSr_{1.82}(PO_4)_2$:0.09Sm^{3+},0.09Li^+ phosphor at 384 K was 76.9% of baseline at 298 K, revealing that the $CaSr_{1.82}(PO_4)_2$:0.09Sm^{3+},0.09Li^+ phosphors have good thermal stability. None of the samples had a temperature-induced shift in emission, which confirms the stable chromaticity coordinates of $CaSr_{1.82}(PO_4)_2$:0.09Sm^{3+},0.09Li^+ phosphors.

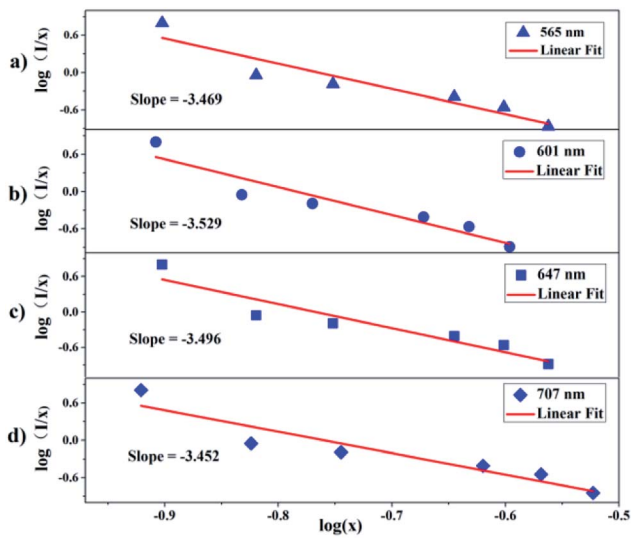

Fig. 9 Relationship between the log(I/x) and log(x) of Sm^{3+} content in the $CaSr_{2-2x}(PO_4)_2$:xSm^{3+},xLi^+ phosphors beyond the quenching concentration, for the peaks at 565 nm (a), 601 nm (b), 647 nm (c) and 707 nm (d).

3.5. Luminescence decay curves and chromaticity coordinates

Fig. 11 shows the decay curves of Sm^{3+} emission for $CaSr_{2-2x}(PO_4)_2$:xSm^{3+},xLi^+ (x = 0.01, 0.06, 0.12 and 0.18) samples excited at 403 nm and monitored at 601 nm. All decay curves can be well fitted to a bi-exponential decay equation as follows:[29,30]

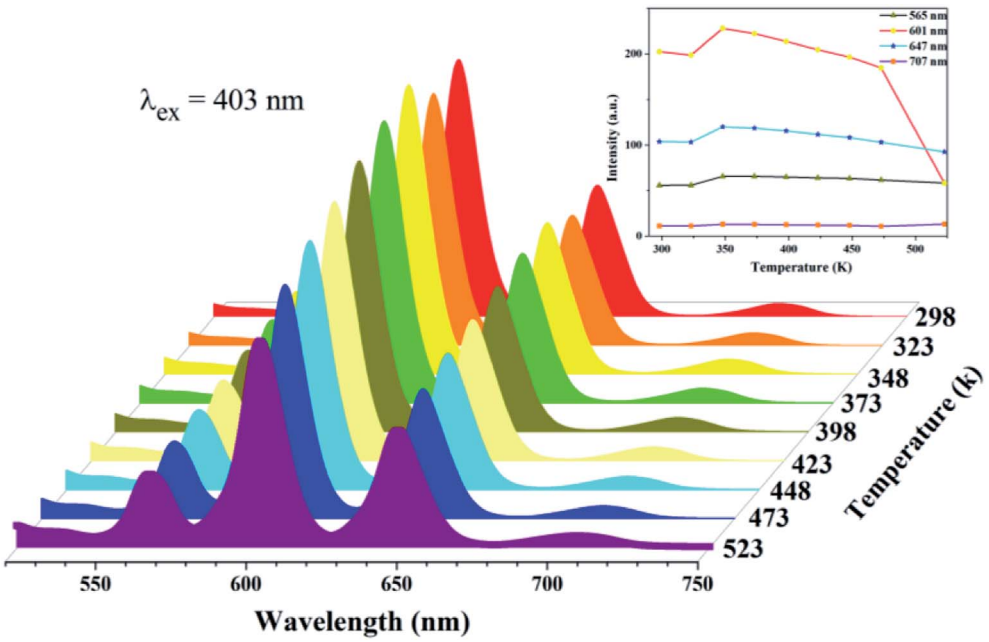

Fig. 10 The temperature-dependent emission spectra of the $CaSr_{1.82}(PO_4)_2$:0.09Sm^{3+},0.09Li^+ phosphor, in the temperature range of 298–523 K, under the excitation of 403 nm; the inset shows the relative emission intensities at 565, 601, 647 and 707 nm as a function of temperature.

$$I(t) = A_1 \exp(-t/\tau_1) + A_2 \exp(-t/\tau_2), \quad (3)$$

where I is the luminescence intensity at time t, A_1 and A_2 are amplitudes, and τ_1 and τ_2 are the luminescence lifetimes. The average emission lifetimes ($\tau_{average}$) were calculated to be 1.14, 0.55, 0.33, and 0.17 ms for $CaSr_{2-2x}(PO_4)_2$:$x$$Sm^{3+}$,$x$$Li^+$ with x = 0.06, 0.12, 0.18, and 0.24, respectively. Table 1 shows the calculated values of lifetimes and fitting parameters. Due to the decreasing distance between Sm^{3+}–Sm^{3+} ions—and the resulting enhanced probability of energy transfer to luminescence killer sites—the emission lifetimes gradually shorten with increasing Sm^{3+} concentration. Thereby, the luminescence lifetimes of Sm^{3+} ions are shortened due to the favorable non-radiative energy transfer processes when the Sm^{3+} concentration increases. Importantly, the contribution of the long-lived component ($\tau_1 \approx 1.25$–0.23 ms) decreases from about 65% to 22% with increasing Sm^{3+} concentration whereas the contribution of the short-lived component ($\tau_2 \approx 0.33$–0.03 ms) increases accordingly. This could be because of the non-equal occupation of the cation sites by the emitting activator Sm^{3+} that has a concentration-dependent preferential occupation in one of the sites as well.

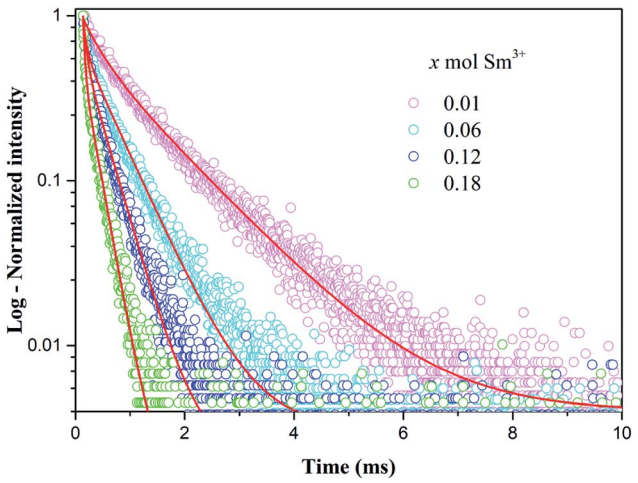

Fig. 11 Decay curves of Sm^{3+} emission in $CaSr_{2-2x}(PO_4)_2$:$x$$Sm^{3+}$,$x$$Li^+$ (x = 0.01, 0.06, 0.12 and 0.18) phosphors, measured at room temperature, under excitation at 403 nm and monitored at 601 nm.

The chromaticity diagram and Commission International de l'Eclairage (CIE) coordinates are very important because they indicate the exact emission color and color purity of the sample.[31] The CIE chromaticity coordinates and the digital image of the $CaSr_{1.82}(PO_4)_2$:0.09Sm^{3+},0.09Li^+ phosphor excited at 403 nm are presented in Fig. 12. The CIE chromaticity coordinates (x, y) of the phosphor were calculated to be (0.5668, 0.3904). They are located in the red region, which is consistent with the observed emission color of the phosphor under 403 nm excitation. Therefore, the $CaSr_{2-2x}(PO_4)_2$:$x$$Sm^{3+}$,$x$$Li^+$ material can be used as a red phosphor for w-LEDs in solid-state lighting applications.

Table 1 Determined luminescence lifetimes and fitting parameters for the $CaSr_{2-2x}(PO_4)_2$:$x$$Sm^{3+}$,$x$$Li^+$ (x = 0.01, 0.06, 0.12 and 0.18) samples

x	τ_1 (ms)	A_1 (%)	τ_2 (ms)	A_2 (%)	$\tau_{average}$ (ms)	R^2
0.01	1.25	65.7	0.33	34.3	1.14	0.995
0.06	0.59	60.7	0.07	39.3	0.55	0.996
0.12	0.37	50.4	0.05	49.6	0.33	0.994
0.18	0.23	22.2	0.03	77.8	0.17	0.993

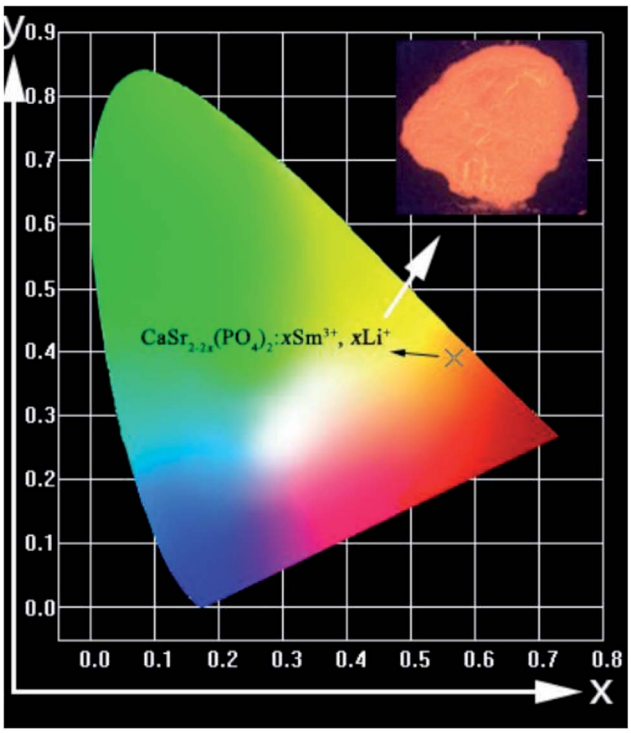

Fig. 12 Color coordinates for $CaSr_{1.82}(PO_4)_2$:0.09Sm^{3+},0.09Li^+ material, in the CIE chromaticity diagram; the inset shows a digital photograph of the red-emitting phosphor excited at 403 nm.

4. Conclusions

In summary, a series of $CaSr_{2-2x}(PO_4)_2$:xSm^{3+},xLi^+ phosphors were prepared for the first time by a conventional solid-state reaction. The phase structure, luminescence properties, thermal quenching, and emission decay curves were investigated. XRD patterns showed that the phosphor can be indexed to hexagonal apatite structure according to the results of crystal structure refinement. Under 403 nm excitation, the $CaSr_{2-2x}(PO_4)_2$:xSm^{3+},xLi^+ phosphors showed four emission bands centered at 565, 601, 647, and 707 nm. The excitation spectra showed narrow excitation bands from 250 to 550 nm with a maximum at 403 nm. This means that the phosphor can be effectively excited by UV chips for potential applications in w-LEDs. The optimum dopant concentration of Sm^{3+} ions is 0.09. Furthermore, the quenching mechanism between the Sm^{3+} ions was recognized as quadrupole–quadrupole (q–q) interactions. The dependence of the emission spectra on temperature indicated that the phosphor has a good thermal stability in both emission color and intensity. The CIE chromaticity coordinates of the selected $CaSr_{2-2x}(PO_4)_2$:xSm^{3+},xLi^+ sample were calculated to be (0.5668, 0.3904); they are located in the red-light region. These results indicated that $CaSr_{2-2x}(PO_4)_2$:xSm^{3+},xLi^+ phosphors have good potential for use as red-emitting luminophores for phosphor-converted w-LEDs.

Conflicts of interest

There are no conflicts to declare.

Acknowledgements

The present work is supported by the National Natural Science Foundation of China (Grant No. 41802040). Yuying Chen also thanks to the College Student Research Innovation Program of China University of Geosciences, Beijing.

References

1 Q. F. Guo, Q. D. Wang, L. W. Jiang, L. B. Liao, H. K. Liu and M. F. Mei, *Phys. Chem. Chem. Phys.*, 2016, **118**, 15545–15554.
2 X. X. Ma, L. B. Liao, Q. F. Guo, H. K. Liu, T. S. Zhou and L. F. Mei, *RSC Adv.*, 2018, **8**, 27332–27341.
3 Y. L. Zhu, Y. J. Liang, M. F. Zhang, M. H. Tong, G. G. Li and S. Wang, *RSC Adv.*, 2015, **5**, 98350–98360.
4 H. K. Liu, L. B. Liao, Q. F. Guo, D. Yang and L. F. Mei, *J. Lumin.*, 2017, **181**, 407–410.
5 M. F. Zhang, Y. J. Liang, R. Tang, D. Y. Yu, M. H. Tong, Q. Wang, Y. L. Zhu, X. Y. Wu and G. G. Li, *RSC Adv.*, 2014, **4**, 40626–40637.
6 G. G. Li, Y. Zhao, Y. Wei, Y. Tian, Z. W. Quan and J. Lin, *Chem. Commun.*, 2016, **52**, 3376–3379.
7 A. Shyichuk, R. T. Moura Jr, A. N. C. Neto, M. Runowski, M. Zarad, A. Szczeszak, S. Lis and O. L. Malta, *J. Phys. Chem. C*, 2016, **120**, 28497–28508.
8 M. Runowski, J. j. Marciniak, T. Grzyb, D. Przybylska, A. Shyichuk, B. Barszcz, A. Katrusiak, S. Lis, A. Katrusiak and S. Lis, *Nanoscale*, 2017, **9**, 16030–16037.
9 M. Runowski, S. Goderski, J. Paczesny, M. Księżopolska-Gocalska, A. Ekner-Grzyb, T. Grzyb, J. D. Rybka, M. Giersig and S. Lis, *J. Phys. Chem. C*, 2016, **120**, 23788–23798.
10 W. J. Tang and Z. Zhang, *J. Mater. Chem. C*, 2015, **3**, 5339–5346.
11 K. Li, D. L. Geng, M. M. Shang, Y. Zhang, H. Z. Lian and J. Lin, *J. Phys. Chem. C*, 2014, **118**, 11026–11034.
12 H. Ji, Z. Huang, Z. Xia, M. S. Molokeev, V. V. Atuchin and S. Huang, *Inorg. Chem.*, 2014, **53**, 11119–11124.
13 J. Zhang, J. M. Jia and Z. H. Hua, *Mater. Des.*, 2015, **87**, 124–129.
14 H. P. Ji, Z. H. Huang, Z. G. Xia, M. S. Molokeev, V. V. Atuchin, M. H. Fang and S. F. Huang, *Inorg. Chem.*, 2014, **53**, 5129–5135.
15 H. Ye, M. Y. He, T. S. Zhou, Q. F. Guo, J. L. Zhang, L. B. Liao, L. F. Mei, H. K. Liu and M. Runowski, *J. Alloys Compd.*, 2018, **757**, 79–86.
16 B. Ma, X. Q. Ma, T. H. Xu, K. Su and Q. X. Zhang, *RSC Adv.*, 2018, **8**, 14164–14169.
17 Q. F. Guo, C. L. Zhao, L. B. Liao, S. Lis, H. K. Liu, L. F. Mei and Z. Q. Jiang, *J. Am. Ceram. Soc.*, 2017, **100**, 1–11.
18 L. Li, X. H. Tang, Z. Q. Jiang, X. J. Zhou, S. Jiang, X. B. Luo, G. T. Xiang and K. N. Zhou, *J. Alloys Compd.*, 2017, **701**, 515–523.
19 T. S. Zhou, L. F. Mei, Y. Y. Zhang, L. B. Liao, H. K. Liu and Q. F. Guo, *Opt. Laser Technol.*, 2019, **111**, 191–195.
20 X. Y. Huang and H. Guo, *Ceram. Int.*, 2018, **44**, 10340–10344.

21 R. Yu, H. Mi Noh, B. Kee Moon, B. Chun Choi, J. Hyun Jeong, H. Sueb Lee, K. Jang and S. Soo Yi, *J. Lumin.*, 2014, **152**, 133–137.
22 Y. Zhang, B. Ding, L. Yin, J. Xin, R. Zhao, S. Zheng and X. Yan, *Inorg. Chem.*, 2018, **57**, 507–518.
23 G. Blasse, *Philips Res. Rep.*, 1969, **24**, 131–144.
24 D. L. Dexter and J. H. Schulman, *J. Chem. Phys.*, 1954, **22**, 1063–1070.
25 L. G. Van Uitert, *J. Electrochem. Soc.*, 1967, **114**, 1048–1053.
26 J. Xu, Z. H. Ju, X. P. Gao, Y. Q. An, X. L. Tang and W. S. Liu, *Inorg. Chem.*, 2013, **52**, 13875–13881.
27 T. Takeda, N. Hirosaki, S. Funahshi and R. Xie, *Chem. Mater.*, 2015, **27**, 5892–5898.
28 J. J. Chen, Y. Zhao, Z. Y. Mao, D. J. Wang and L. J. Bie, *J. Lumin.*, 2017, **186**, 72–76.
29 C. H. Huang and T. M. Chen, *J. Phys. Chem. C*, 2011, **115**, 2349–2355.
30 R. Vijayakumar, H. Guo and X. Y. Huang, *Dyes Pigm.*, 2018, **156**, 8–16.
31 J. S. Kumar, K. Pavani, A. M. Babu, N. K. Giri, S. B. Rai and L. R. Moorthy, *J. Lumin.*, 2010, **130**, 1916–1923.